Mechanistic insights into the *ortho*-defluorination-hydroxylation of *2*-halophenolates promoted by a bis(μ-oxo)dicopper(III) complex

Pau Besalú-Sala,‡ Carla Magallón,‡ Miquel Costas,* Anna Company,* Josep M. Luis*

Institut de Química Computacional i Catàlisi and Departament de Química, Universitat de Girona, C/Maria Aurèlia Capmany 69, 17003, Girona, Catalonia, Spain

Keywords: C-F activation, O_2 activation, $[Cu_2O_2]^{2+}$, DLPNO-CCSD(T), DFT

ABSTRACT: C–F bonds are one of the most inert functionalities. Nevertheless, some $[Cu_2O_2]^{2+}$ species are able to defluorinate-hydroxylate *ortho*-fluorophenolates in a chemoselective manner over other *ortho*-halophenolates. Albeit it is known that such reactivity is promoted by an electrophilic attack of a $[Cu_2O_2]^{2+}$ core over the arene ring, the crucial details of the mechanism that explain the chemo and regioselectivity of the reaction species remain unknown, and it has not being determined either if $Cu^{II}_2(\eta^2:\eta^2\text{-}O_2)$ or $Cu^{III}_2(\mu\text{-}O)_2$ species are responsible for the initial attack on the arene. Herein, we present a combined theoretical and experimental mechanistic study to unravel the origin of the chemo-selectivity of the ortho-defluorination-hydroxylation of 2-halophenolates by the $[Cu_2(O)_2(DBED)_2]^{2+}$ complex. Our results show that the equilibria between (side-on)peroxo (**P**) and bis(μ-oxo) (**O**) isomers plays a key role in the mechanism, being the latter the reactive species. Furthermore, on the basis of quantum mechanical calculations, we have been able to rationalize the chemoselective preference of $[Cu_2(O)_2(DBED)_2]^{2+}$ catalyst for the C–F activation over C–Cl and C–H activations.

INTRODUCTION

The high electronegativity of fluorine strongly polarizes and shortens C–F bonds, reinforcing the ionic component of the chemical bond. As consequence, the C–F has the largest C–X (X=F, Cl, Br, I) dissociation energy (up to 130 kcal·mol^{-1}).[1] Thus, C–F is considered the most inert organic functionality, which confers a high thermal stability to the fluorinated organic compounds. Due to the increment of the lipophilicity caused by the fluorination, fluorinated drugs present larger *in vivo* residence times than their non-fluorinated counterparts.[2, 3] Therefore, fluorinated compounds are of great interest in medicinal chemistry and agrochemistry.[2] On the other hand, fluorinated compounds are also currently in the spotlight since their metabolization is very difficult due to the aforementioned high stability, which triggers their bioaccumulation and environmental persistence. This scenario pops up a dilemma since we are facing two sides of the same coin. The particular properties of fluorinated organic molecules make them interesting for medicinal chemistry or agrochemistry. However, they are also responsible for their bioaccumulation and biomagnification.[4, 5] Therefore, finding strategies to promote activation and subsequent transformation of C–F bonds into more reactive functionalities is the key to facilitate the degradation of the fluorinated organic molecules.

In nature, aliphatic and aromatic fluorinated compounds can be enzymatically functionalized. In particular, the defluorination of aromatics occurs in cytochrome P450, chloroperoxidase and FAD-containing phenol hydroxylases, which can convert 2-fluorophenols into the corresponding chatecols.[6-8] On the contrary, tyrosinase, which is efficient in the ortho-hydroxylation of phenols, cannot *ortho*-defluorinate-hydroxylate 2-fluorophenols.[9, 10] Indeed, 2-flurophenols inhibit the catalytic activity of tyrosinase. The active species of this enzyme consists on a (η^2:η^2-peroxo)dicopper (II) species (**P**) which is able to hydroxylate phenols through an electrophilic aromatic substitution. Some of us have shown that bioinspired systems such as $[Cu^{III}_2(\mu\text{-}O)_2(m\text{-}XYL^{MeAN})]^{2+}$ and $[Cu_2(\mu\text{-}\eta^2\text{:}\eta^2\text{-}O_2)(OBED)_2]^{2+}$ (Figure 1) elicit the hydroxylation-defluorination of 2-fluorophenolates to give the corresponding catechols.[11] In contrast, other model systems such as $[Cu_2(\mu\text{-}\eta^2\text{:}\eta^2\text{-}O_2)(L^{Py2Bz})_2]^{2+}$ are unable to cleave the C–F bond. Although the peroxo (**P**) species is the most stable isomer of both $[Cu_2(\mu\text{-}\eta^2\text{:}\eta^2\text{-}O_2)(OBED)_2]^{2+}$ and $[Cu_2(\mu\text{-}\eta^2\text{:}\eta^2\text{-}O_2)(L^{Py2Bz})_2]^{2+}$, the former is in equilibrium with the bis(μ-oxo)dicopper(III) (**O**) isomer. This led us to consider that the latter isomer is the active species in the defluorination of 2-fluorophenols (Figure 1).[12, 13, 14]

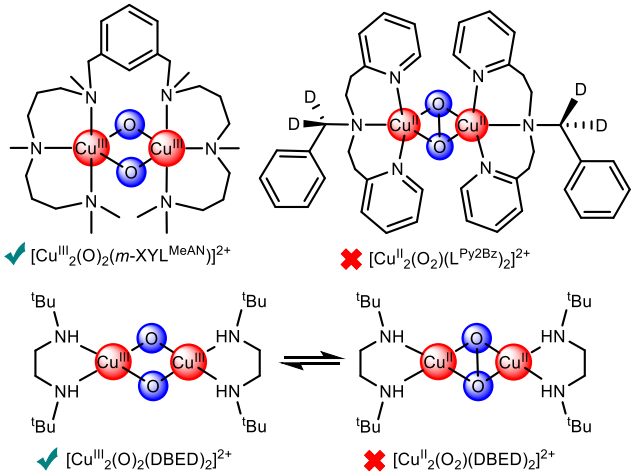

Figure 1. Three Cu_2O_2-based species. Tick marks indicate that defluorination-hydroxylation products are obtained, whereas the red cross indicates the opposite.

In the case of $[Cu^{III}_2(\mu\text{-}O)_2(m\text{-}XYL^{MeAN})]^{2+}$ only the **O** isomer is observed,[15] further supporting the idea that this isomer is the only competent to carry out the defluorination reaction.[11] Of relevance to these observations, high valent iron-oxo and iron manganese species have also shown analogous reactivity.[16-20] In addition, de Visser and co-workers showed that a μ-nitrido diiron phthalocyanine complex is able to activate and hydroxylate the C-F bonds of hexafluorobenzene derivatives.[21]

In this work, theory and experiments are combined to determine the details of the mechanism of the selective ortho-hydroxylation–defluorination of 2-fluorophenolates with $[Cu_2O_2(DBED)_2]^{2+}$ (**1**), a compound first described by Stack and co-workers.[12, 13] Specifically, our study was directed to address the following questions; to unravel which is the actual defluorination-oxygenation agent, either **P** or **O** species, ($\mathbf{1^P}$ and $\mathbf{1^O}$, Figure 2). Both isomers have been experimentally detected for this system: The **P** isomer is generated upon reaction of the copper(I) precursor with O_2, while the **O** compound is experimentally detected upon coordination of a phenolic substrate to **P**. A second aspect to clarify is the origin of the selective oxygenation at the *ortho* C–F over the *ortho* C–H position in the reaction with 2-fluorophenols, despite the former was devised as more electron poor than the latter. Finally, the study aimed at explaining while C–Cl bonds, weaker than C–F bonds, remain unreactive.

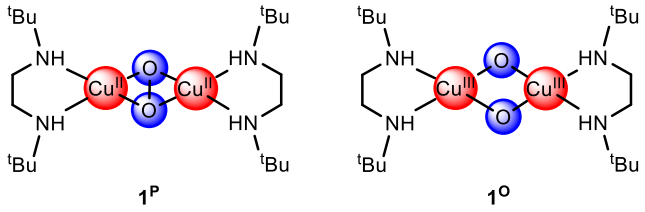

Figure 2. Schematic representation of the two studied isomers of $[Cu_2O_2(DBED)_2]^{2+}$ (**1**): the (η^2:η^2-peroxo)dicopper(II) species, ($\mathbf{1^P}$, left) and the bis(μ-oxo)dicopper(III) species, ($\mathbf{1^O}$, right).

COMPUTATIONAL DETAILS

The computationally-aided modelling of $[Cu_2O_2]^{2+}$-based compounds for the defluorination-hydroxylation of fluorophenols has been exploited in the last decade, yet is not an easy task.[22-25] Due to the high number of electrons that must be correlated, multireference methods have not been extensively used to study $[Cu_2O_2]^{2+}$ reactivity. Density functional theory (DFT) arises as a powerful alternative to study these compounds due to its good accuracy/cost balance.[26, 27] However, some important considerations must be taken into account. In particular, and of high interest for the current manuscript, is that an unequivocal characterization of $[Cu_2O_2]^{2+}$ isomerization equilibria is certainly quite difficult to achieve by DFT means.[26, 28, 29] Whereas (end-on)peroxo/(side-on)peroxo isomerization equilibria is usually well described by hybrid functionals, (side-on)peroxo/bis(μ-oxo) (**P**/**O**) equilibria presented by **1** is better described by pure functionals.[30] Hybrid functionals tend to under-stabilize bis(μ-oxo) species, being the magnitude of the under-stabilization proportional to the amount of exact exchange introduced in the functional definition. Therefore, we have performed the DFT calculations using a pure functional. Nevertheless, the DFT results of the **P**/**O** equilibria**,** which have a key relevance in the present manuscript, were improved with DLPNO-CCSD(T) calculations, which produces more reliable predictions than DFT.[31-34]

DFT electronic structure calculations were performed with Gaussian 09 software package[35] using the spin-unrestricted UM06-L[36] density functional. For the geometric optimizations the molecular orbitals were spanned into the Pople-type 6-311G(d) basis set[37, 38] (Method A). Singlet (both open and closed shell) and triplet spin symmetries were explored, reporting always the most stable one. The nature of the stationary points was determined by analytical frequency calculations. To compute subsequent Gibbs free energy corrections, the temperature was set up at 183.15K to simulate the experimental conditions. Furthermore, the connection between TS and intermediates was unambiguously stablished by intrinsic reaction path calculations (IRC),[39] using the local quadratic approximation to determine the prediction step.[40] All DFT energy values were systematically improved by evaluating the electronic structures of the optimized geometries using the Dunning's correlation consistent triple-ζ basis set cc-pVTZ, suppressing the functions with higher angular momentum only for the Cu atoms (cc-pVTZ-g)[41, 42] and introducing solvation (acetone) effects through SMD model (Method B).[43] Spin-contamination was removed if necessary by using the following expressions:[26, 44, 45]

$$E_{spin-corr} = \frac{E_S - aE_{(S+1)}}{1-a} \quad (1)$$

$$a = \frac{\langle S_S{}^2 \rangle - S\cdot(S+1)}{\langle S_{(S+1)}{}^2 \rangle - S\cdot(S+1)} \quad (2)$$

where E_S and $E_{(S+1)}$ are the broken-symmetry DFT energies for the S and S+1 spin states, respectively, obtained at UM06-L/cc-pVTZ-g~SMD level of theory. $\langle S_s{}^2 \rangle$ and $\langle S_{(s+1)}{}^2 \rangle$ are the expectation values of the square total spin momentum obtained at the same level of theory for the S and S+1 spin states, respectively. And $E_{spin-corr}$ is the spin-corrected DFT electronic energy. In this manner, *a* parameter takes into account the amount of spin contamination on S state due to S+1 state.

ORCA 4.1.0 software package[46] was used for the domain-local pair natural orbitals coupled cluster with singles, doubles and perturbative triples, DLPNO-CCSD(T), single point energy calculations, together with cc-pVTZ basis set (and cc-pVTZ as auxiliary basis) and SMD solvent corrections. TightPNO cutoffs were set for the transformation of the orbitals into the DLPNOs. TightSCF criterion was set for the convergence of the SCF and the CC iterations.

The values of T1 diagnostic of all DLPNO-CCSD calculations were always lower than 0.024, indicating that most of the correlation energy is captured by DLPNO-CCSD(T) method. Therefore, there is no evidence of requiring multi-referential calculations to obtain a good description of the studied species.

RESULTS AND DISCUSSION

In order to address the questions described at the end of the introduction, we have performed a detailed computational study of the *ortho*-defluorination-hydroxylation mechanism of 2-fluorophenolate and 2,6-difluorophenolate promoted by **1**.

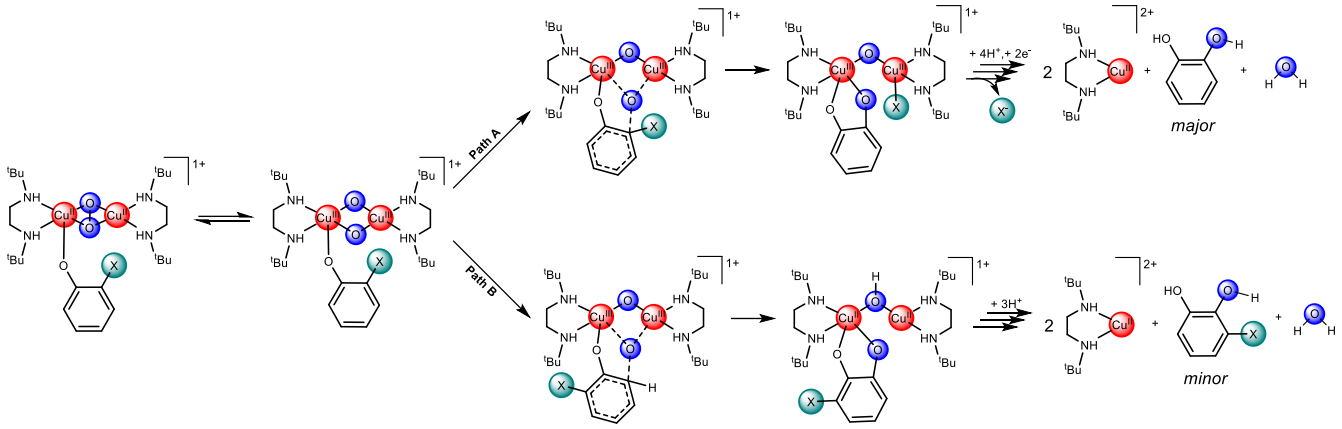

Figure 3. Schematic representation of the *ortho*-defluorination-hydroxylation reaction mechanism (Path A) and the competing *ortho*-hydroxylation reaction mechanism (Path B). The proton source in final steps is $HClO_4$ (0.5M). In the path A, the source of electrons of the last step is given by an external reducing agent (ascorbate or Zn powder),[11] or in its absence, by an intermolecular decomposition of a second Cu_2O_2 complex.

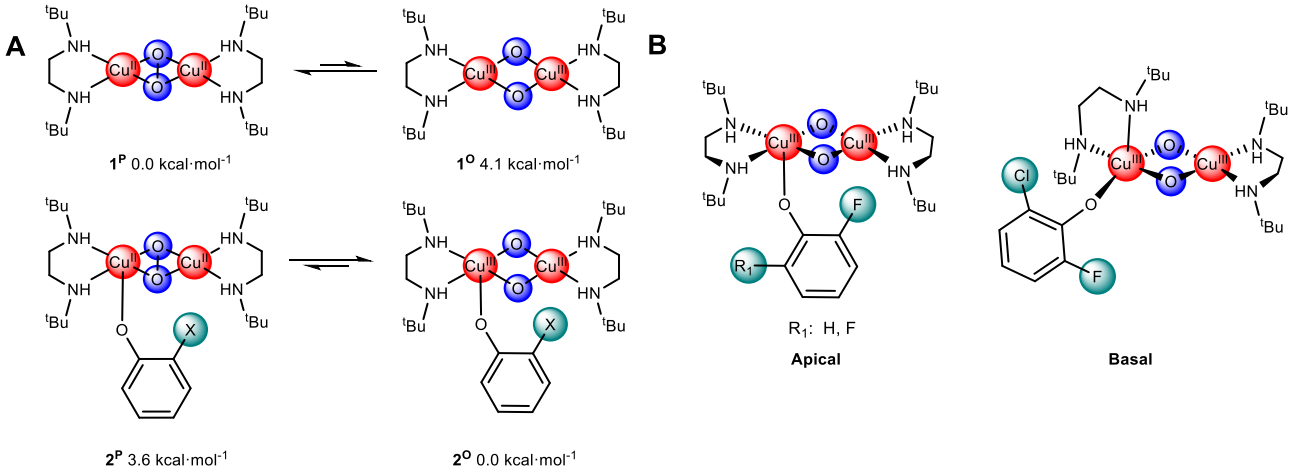

Figure 4. **A** Relative stability (kcal·mol^{-1}) of $\mathbf{1^P}$/$\mathbf{1^O}$ and $\mathbf{2^P}$/$\mathbf{2^O}$ computed at DLPNO-CCSD(T)/cc-pVTZ~SMD//M06-L/6-331G(d) level. **B** Reactive $\mathbf{2^O}$ conformers for 2-fluorophenolate and 2,6-difluorophenolate (apical coordination), and 6-chloro-2-fluorophenolate (basal coordination).

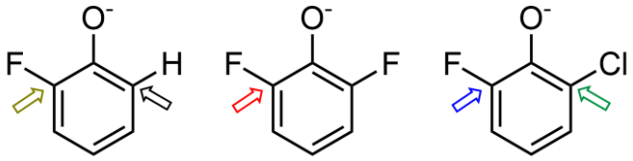

Figure 5. Five possible attacks studied in this manuscript over 2-fluorophenolate, 2,6-difluorophenolate and 6-chloro-2-fluorophenolate.

Furthermore, we investigated the chemo-selectivity that **1** exhibits on the C–F bond activation over C–H or C–Cl bond activations for 2-fluorophenolate and 2-chloro-6-fluorophenolate. Therefore, a total of 5 different possible reaction paths were studied (Figure 5).

The proposed mechanism of *ortho*-defluorination-hydroxylation of 2-fluorophenolate compounds carried out by **1** presents two principal steps (Figure 3). The first main step is the electrophilic attack of the $[Cu_2O_2]^{2+}$ core to the aromatic ring, that implies the pyramidalization of the attacked carbon. This C–X activation can occur at each of the two phenolate *ortho* positions, giving two possible reaction paths, Path A or Path B, which will be indicated using either A or B subscripts in the name of the intermediates and TSs. The second main step is given by the rearomatization of the substrate that leads to the catechol product either by the transfer of the halogen to one of the metals (Path A, *ortho*-defluorination-hydroxylation reaction), or through the proton abstraction by the remaining oxygen atom of the core (Path B, ortho-hydroxylation). Path A has some important differences with respect to the mechanism of defluorination-hydroxylation of hexafluorobenzene catalyzed by a μ-nitrido diiron phthalocyanine complex. In the latter case a ketone intermediate is formed after a 1,2-fluoride shift and only one transition metal is involved in the C-F activation.[21] However, in both defluorination-hydroxylation mechanisms the rearomatization of the ring plays a key role.

1 is formed *in situ* by the reaction of $[Cu^I(DBED)(CH_3CN)]^{1+}$ and atmospheric oxygen.[11] Although the most stable isomer is the species $\mathbf{1^P}$, this compound may be in equilibrium with its bis(μ-oxo)dicopper(III) isomer, $\mathbf{1^O}$. The first requirement to elucidate the reaction mechanism is to determine which is the actual reactive species, $\mathbf{1^P}$ or $\mathbf{1^O}$. Spectroscopic monitoring of the reaction of $\mathbf{1^P}$ with fluorophenolates (*vide infra*) reveals that it proceeds via an initial phenolate binding to one of the copper atoms. Consequently, using 2-fluorophenolate as a model substrate, we computed the relative Gibbs energies of **P** and **O** isomers either without ($\mathbf{1^P}$/$\mathbf{1^O}$) or with ($\mathbf{2^P}$/$\mathbf{2^O}$)

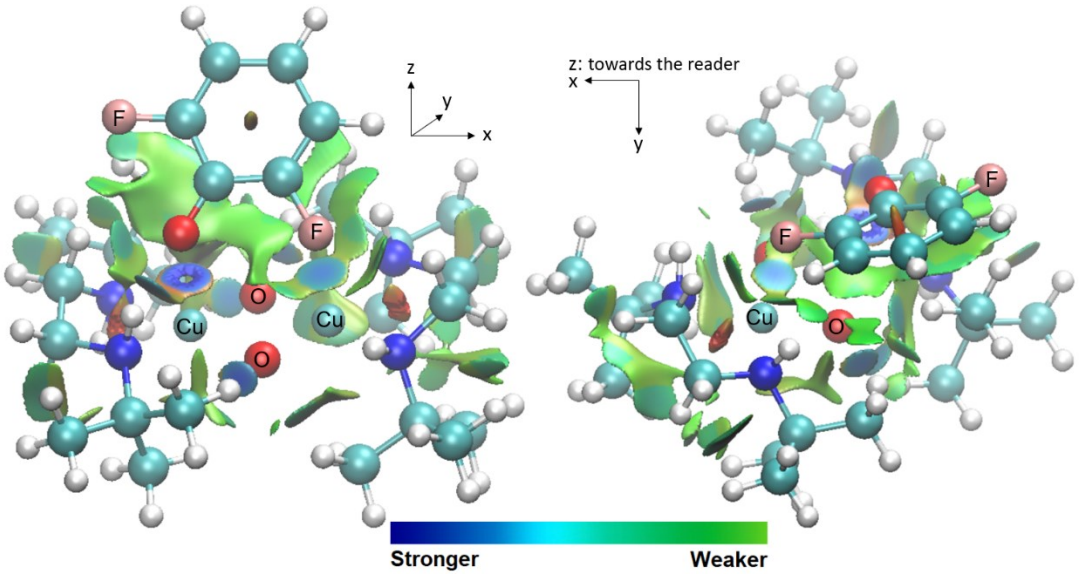

Figure 6. Two different views of the non-covalent attractive interaction isosurfaces generated by NCIPLOT for **3**$_{FF}$ intermediate.

2-fluorophenolatecoordinated to the complex at DLPNO-CCSD(T)/cc-pVTZ~SMD//M06-L/6-331G(d) level of theory. In absence of substrate, **1**^{P} species is 4.1 kcal·mol^{-1} more stable than **1**^{O}. However, upon substrate coordination, this behavior is reversed and **2**^{O} becomes 3.6 kcal·mol^{-1} more stable than **2**^{P} (Figure 4A). These results are in line with those previously described by Stack and coworkers, indicating that conversion to the **O** isomer occurs when **P** coordinates to a phenolic substrate.[12]

Thus, DLPNO-CCSD(T) single point calculations agree with the experimental observation that when the Cu_2O_2 species is generated by reaction of the copper(I) precursor $[Cu^{I}(DBED)(CH_3CN)]^{+}$ with O_2, the main isomer is **1**^{P}. However, upon addition of the phenolic substrate in the reaction mixture, the equilibrium is shifted towards **2**^{O}. Therefore, we placed the focus of our study on the **2**^{O} species, although both **2**^{O} and **2**^{P} isomers were considered as possible active species of the reaction mechanism.

It is worth highlighting that for all fluorophenolate substrates studied both apical and basal coordination motifs (with respect to the N_2CuO_2 plane) were explored and, in all cases, the former was the most stable. However, for the particular case of the attack over the position 6 of 6-chloro-2-fluorophenolate, we were only able to find the transition state corresponding to the electrophilic attack for the isomer presenting basal coordination (Figure 4B). In this case, the activation barrier corresponding to the C-F activation, the reaction observed experimentally, is smaller than the barrier associated with a hypothetical C-Cl cleavage, which therefore is irrelevant.

The first step of the reaction corresponds to a non-covalent attractive interaction between the reactive halogen (F or Cl) with the less coordinatively-saturated Cu, giving intermediate **3**. Within crystal field theory, for a square-planar Cu(III) center, all *d* orbitals are occupied but the $d_{x^2-y^2}$, which does not have the proper symmetry to form an apical bond. Therefore, combination of the d_{z^2} of the Cu(III) and one lone pair of the halogen leads to a non-bonding covalent interaction. However, there exists a non-covalent attractive interaction between the halogen and the Cu(III), as it can be seen in attractive interaction isosurfaces generated by the NCIPLOT[47, 48] program based on the real-space analysis of the reduced density gradient (see Figure 6 and SI).

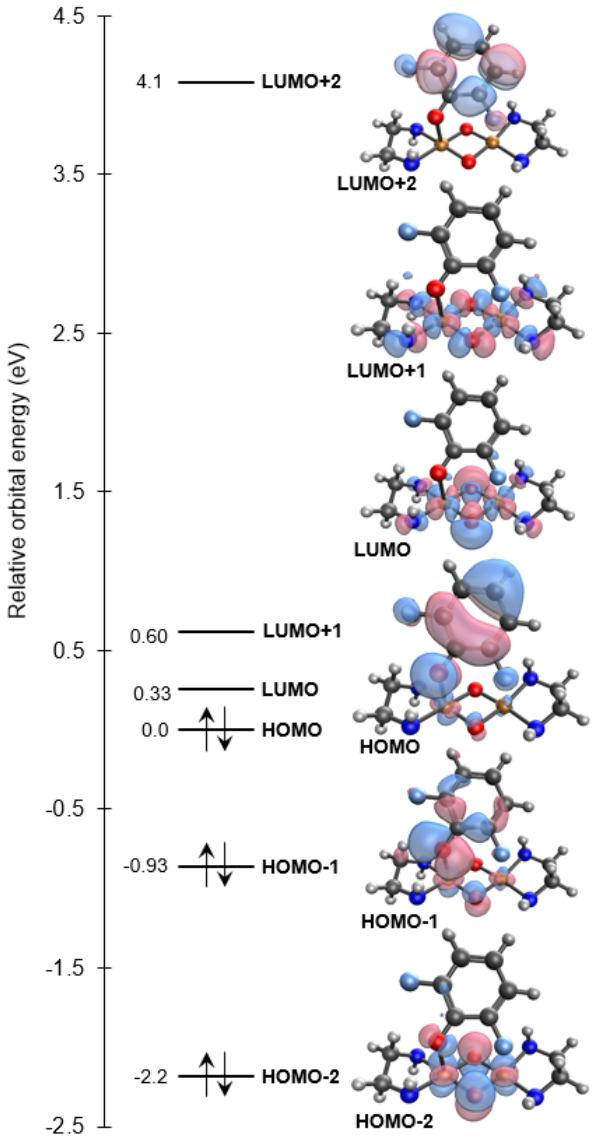

Figure 7. Molecular orbital energy diagram of the six frontier orbitals of **2**$_{F}$. Copper complex simplified for clarity.

Along with the aforementioned Cu–X interaction, the C–X bond is slightly elongated (from 1.35 to 1.38 Å). This key attractive interaction does not exist for the attack at position 6 of 2-fluorophenolate, because the proton obviously does not have a lone pair to interact with the Cu(III). Therefore, for the competing C–H *ortho*-hydroxylation reaction intermediate $\mathbf{3_H}$ does not exist.

For all substrates, the next step of the reaction is an electrophilic attack of the $[Cu_2O_2]^{2+}$ core to the aromatic ring. This attack is ruled by the electrophilic character of the Cu, and therefore it is particularly favored in the bis(μ-oxo)dicopper(III) $\mathbf{2^O}$ isomer compared to the (η²:η²-peroxo)dicopper(II) $\mathbf{2^P}$ species (See SI for details). The HOMO of the intermediate **3** is mainly located over the arene, which agrees with its electrophilic character, while the LUMO is an antibonding orbital mainly placed on the $[Cu_2O_2]^{2+}$ core, which agrees with its nucleophilic character (Figure 7). In the transition state of this step, which corresponds to the rate determining step (r.d.s.) of the reaction, the C–X ($\mathbf{TS1_A}$) or C–H ($\mathbf{TS1_B}$) bond is elongated while the C–O distance is shortened and the attacked carbon of the aromatic ring is pyramidalized. The apical attack of the $[Cu_2O_2]^{2+}$ to the arene cannot be explained only with the participation of the HOMO and LUMO, and for instance the apical attack to the 2,6-difluorophenolate requires the participation of the HOMO-2 and LUMO+2 orbitals. (Figure 7).

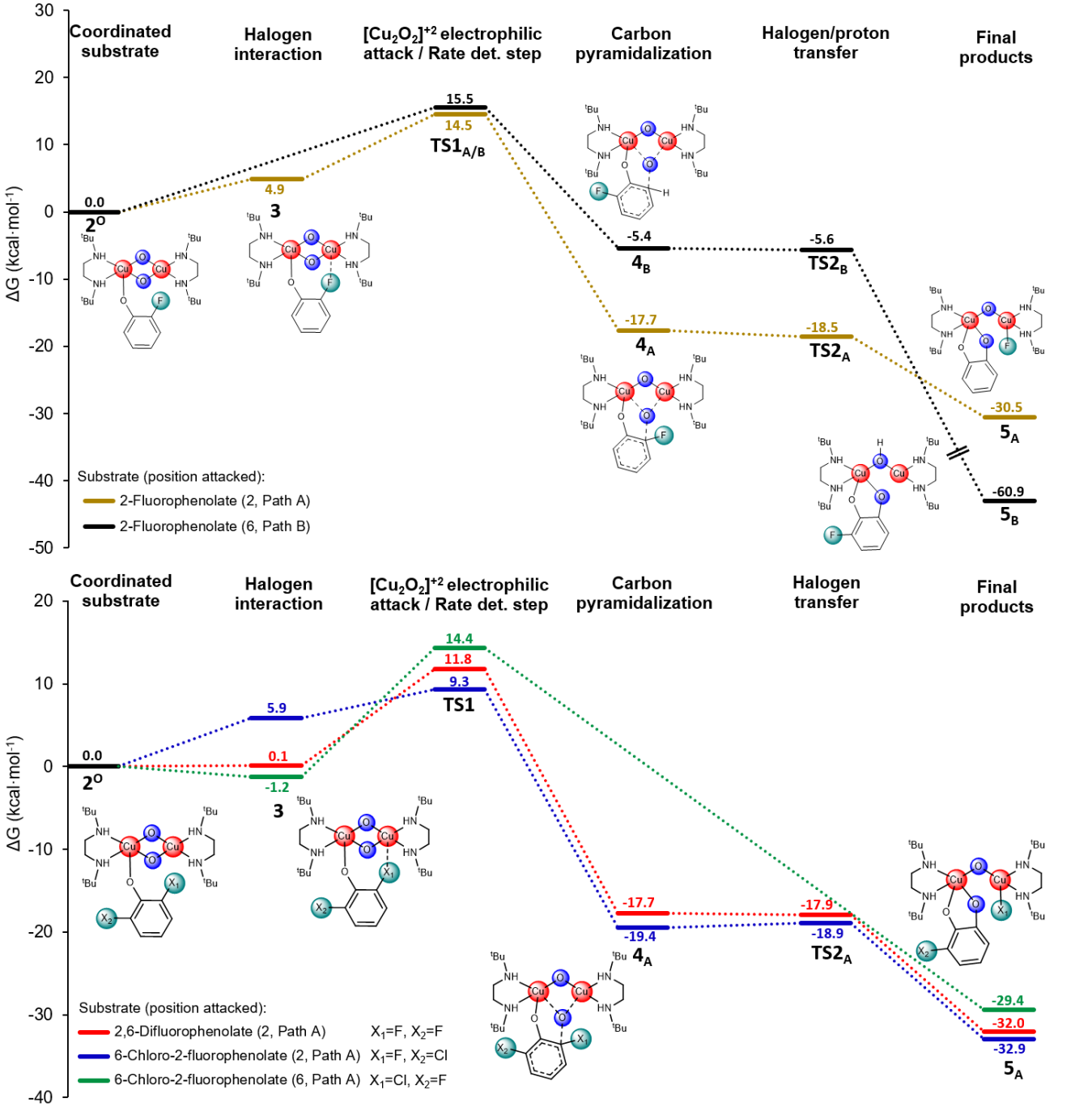

Figure 8. Calculated free-energy profiles at the UM06-L/cc-pVTZ-g~SMD//UM06-L/6-311G(d) level of theory for 2-fluorophenolate (top), 2,6-difluorophenolate and 6-chloro-2-fluorophenolate (bottom) substrates. Gibbs free energies (G, in kcal·mol^{-1}) are relative to $\mathbf{2^O}$.

To confirm the electrophilic nature of the attack of the Cu_2O_2 over the aromatic ring, a Hammett plot was experimentally determined. Compound $\mathbf{1^P}$ was generated at -80 ºC in Me-THF upon reaction of the copper(I) precursor $[Cu(DBED)(CH_3CN)]^+$ with O_2. This process was monitored by UV-vis spectroscopy. Once $\mathbf{1^P}$ was fully formed, the temperature was lowered to -110 ºC and the appropriate amount of sodium 2-fluoro-4-Y-phenolate (Y = Cl, F, H, CH_3) was added. This resulted in the formation of the corresponding $\mathbf{2^O}$ species, in which the bis(μ-oxo) core is bound to the phenolate. Experimental characterization of $\mathbf{2^O}$ was solely done by comparison of the UV-vis spectra with those of analogous species previously generated for *m*-XYL^{MeAN} systems[11] and taking into account that analogous species have been experimentally detected for the DBED system with 2-tert-butyl-4-Y-phenolates.[12] Decay of the UV-Vis spectroscopic features of $\mathbf{2^O}$ showed a first order kinetics and could be adjusted to a single exponential function. The decay rate (*k*) was dependent on the nature of the para-substituent Y. Thus, plotting the logarithm of the decay rate (*k*) as a function of the Hammett parameter of the *para*-substituent (σ_p) resulted in a linear correlation with a negative slope (ρ = -3.5, Figure 9) indicative of an electrophilic attack over the aromatic ring, which agrees with the proposed mechanism based on theoretical calculations. The intermediates $\mathbf{4_A}$ of path A contain a dearomatized ring presenting one nearly-sp^3 carbon bound to both the reactive oxygen from the $[Cu_2O_2]^{2+}$ core and the halogen. This halogen (either Cl or F) is strongly interacting with the closest Cu. For the attack at position 6 of 2-fluorophenolate (path B), intermediate $\mathbf{4_B}$ is generated. This intermediate presents also one nearly-sp^3 carbon, but in this case, it is bound to the reactive oxygen from the $[Cu_2O_2]^{2+}$ core and one proton. The main difference of $\mathbf{4_B}$ with respect to $\mathbf{4_A}$ is that the proton cannot interact with the Cu(III), ultimately determining the reactivity of $\mathbf{4_B}$. Neither $\mathbf{4_A}$ nor $\mathbf{4_B}$ are stable intermediates and quickly rearomatize and evolve to the final product. For path A, such product ($\mathbf{5_A}$) is obtained through a halogen transfer from the aromatic ring to the metal. Due to the inclusion of the entropic and thermal corrections, the Gibbs energy barriers of the halogen transfers are close to zero or even negative, indicating that this step is a barrierless process. Interestingly, for the attack at chlorine position of 2-chloro-6-fluorophenolate, the intermediate $\mathbf{4_A}$ does not exist and $\mathbf{TS1_A}$ evolves directly to products in a concerted asynchronous manner (confirmed by IRC calculations).

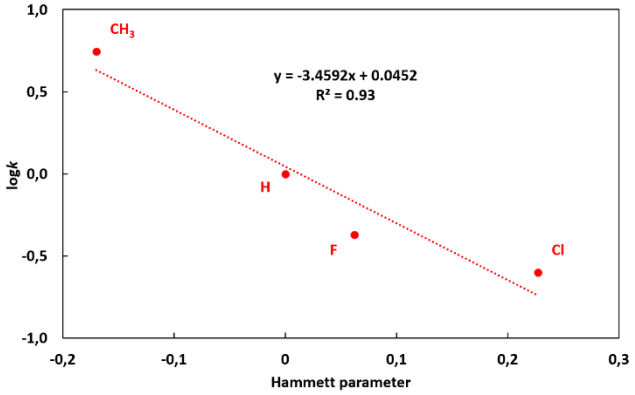

Figure 9. Experimental Hammett plot.

For the alterative *ortho* C–H oxygenation, the mechanism homologous to path A would lead to a Cu–H species, which has not been experimentally detected. Computationally, for 2-fluorophenolate, the formation of the copper hydride is endergonic by 15 kcal·mol^{-1}. Instead, the path B mechanism leads to kinetically and thermodynamically favorable pathway for the *ortho*-hydroxylation of the 2-halophenolates. This path differs from path A at intermediate $\mathbf{4_B}$, which suffers a quasi-barrierless proton transfer to the remaining oxygen of the $[Cu_2O_2]^{2+}$ core forming an OH group. In the transition state of this step ($\mathbf{TS2_B}$) the substrate rearomatizes. To do so, the nearly-sp^3 carbon formed in the previous step has to become sp^2 again, releasing the proton. This proton is very close in space to the remaining O of the $[Cu_2O_2]^{2+}$ core, which ultimately will be transferred to (Figure 8, top). The formation of the final product, $\mathbf{5_B}$ is highly exergonic (*i.e.* ΔG = -60.9 kcal·mol^{-1}).

The computed energy barriers ($\Delta G^{\ddagger}$) determined by **TS1**, from lowest to highest, are 9.3 kcal·mol^{-1} for the C–F activation of 2-chloro-6-fluorophenolate, 11.7 kcal·mol^{-1} for the C–F activation of 2,6-difluorophenolate, 14.5 kcal·mol^{-1} for C–F activation of 2-fluorophenolate, 15.5 kcal·mol^{-1} for the C–H activation of 2-fluorophenolate and 15.6 kcal·mol^{-1} for the C–Cl activation of 2-chloro-6-fluorophenolate. These DFT barriers are in fully agreement with observed chemoselectivities. The attack on fluoride instead of chloride in 2-chloro-6-fluorophenolate is 6.3 kcal·mol^{-1} more favorable, which is in concordance with the fact that experimentally only the *ortho*-defluorination is observed.[11] For case of 2-fluorophenolate substrate, for which both Path A and Path B are possible, the attack on C–F (Path A) is 1 kcal·mol^{-1} more favored compared with the attack on C–H (Path B), again in reasonable agreement with the fact that both products are obtained although the *ortho*-defluorination is the major reaction (18:1 C–F vs C–H oxygenation, 38% total yield).

The precision of the computed reaction barriers was checked by experimentally measuring the decay rate of $\mathbf{2^O}$ formed in the reaction of $\mathbf{1^P}$ with sodium 2,6-difluorophenolate at different temperatures *via* an Eyring plot analysis (see SI for details). The experimentally derived $\Delta G^{\ddagger}_{exp}$ is 11.8±0.6 kcal·mol^{-1}, which is in excellent agreement with the aforementioned computed $\Delta G^{\ddagger}_{calc}$ =11.7 kcal·mol^{-1}. Indeed, the difference between the experimental and theoretical $\Delta G^{\ddagger}$ is far lower than the DFT or experimental errors.

Once the reactivity for the bis(μ-oxo) catalyst was understood, we computationally analyzed whether the η^2:η^2-peroxo species could present the same reactivity. We performed linear transit calculations starting from $\mathbf{2^P}$ and exploring the electrophilic attacks from both oxygens to the aromatic ring at UM06-L/6-311G(d) level.

The energy profiles presented in Figure 10 were obtained performing *relaxed* potential energy surface (PES) scan calculations with respect to C_{sp2}–O distances. Both linear transits were targeting a transition state equivalent to $\mathbf{TS1_A}$. At this level of theory, species $\mathbf{2^P}$ is 7.0 kcal·mol^{-1} higher in energy than $\mathbf{2^O}$, preserving DLPNO-CCSD(T) trends.

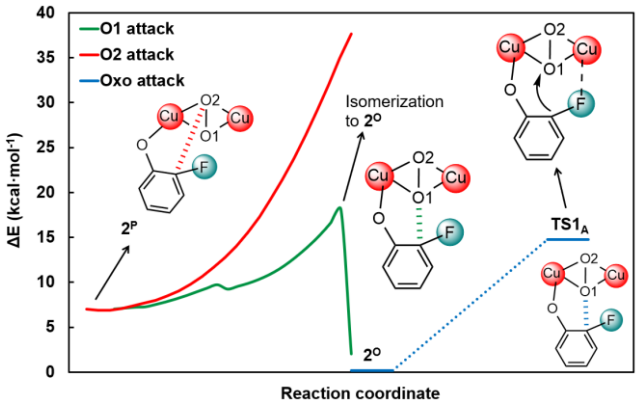

Figure 10. Schematic representation of linear transit calculations starting from **2P** using C–O1 (green) and C–O2 (red) distances as reaction coordinate. DBED ligand omitted for clarity.

In the first linear transit calculation, the O1 is approached to the C of the C–F bond. At the beginning of the relaxed scan the electronic energy increases about 10 kcal·mol^{-1}. However, at the O1–C bond distance of 2.27 Å, there is a significant drop in energy corresponding to the isomerization from distorted **2P** to **2O**. As discussed above, **2O** may evolve until reaching the targeted **TS1A**. Although O2 is not properly located to react with the aromatic ring, we also performed a second linear transit calculation where the O2 is approached to the C of the C–F bond. However, in this relaxed scan the energy rises up about 40 kcal·mol^{-1} without finding a structure similar to **TS1A**. These two linear transit calculations further suggest that only bis(μ-oxo) isomers are able to perform the C–F activation, and then **2P** *should* evolve to **2O** in order to perform the electrophilic attack.

Our results also give theoretical insight about why some compounds such as $[Cu^{III}_2(O)_2(m\text{-}XYL^{MeAN})]^{2+}$ [49] and $[Cu^{II}_2(O_2)(DBED)^2]^{2+}$ (**1**) are able to perform *ortho*-defluorination-hydroxylations, whereas $[Cu^{II}_2(O_2)(L^{Py2Bz})_2]^{2+}$, which has been previously reported by Itoh,[14] does not show up this chemistry. Our computations suggest that *ortho*-defluorination-hydroxylation reactions can only be performed by **O** isomers, which is the most stable species of $[Cu^{III}_2(O)_2(m\text{-}XYL^{MeAN})]^{2+}$ and **2**. On the contrary, the **P** isomer, which is the only populated stable isomer of $[Cu^{II}_2(O_2)(L^{Py2Bz})_2]^{2+}$, is unable to activate the C–F bonds of the aromatic rings. These computational results are in full concordance with the known reactivity of tyrosinase; 2-fluorophenolates are known inhibitors of oxytyrosinase which has been spectroscopically characterized as a pure **P** species. The corresponding **O** isomer has never been detected and is computed to be at least 23 kcal·mol^{-1} higher in energy.[29]

CONCLUSIONS

In this manuscript we have explored the reaction mechanism of the ortho-dehalogenation-hydroxylation of 2-fluorophenolates by combining computational methods and experiments. By using high-level DLPNO-CCSD(T) calculations we have reproduced the experimental description of $[Cu_2O_2(DBED)_2]^{2+}$ (**1**), for which there is an equilibrium between **P** and **O** isomers, shifted towards **O** upon substrate coordination. Our coupled cluster and DFT calculations revealed that **O** is the real executor of the ortho-defluorination-hydroxylation, as it was previously suggested.[11] This fact explains why Cu_2O_2 complexes, for which only the **P** isomer is stable, are unable to perform defluorination-hydroxylation reactions, and also suggests a plausible reason why tyrosinase is inhibited by 2-fluorophenols.

The full reaction mechanism was determined for three substrates (2-fluorophenolate, 2,6-difluorophenolate and 2-chloro-6-fluorophenolate) exploring attacks of the Cu_2O_2 core at 2 and 6 positions. Thus, we took into account also the possibility of having a competing hydroxylation over a C–H bond (Path B). In all cases, the attack of one oxygen of the $[Cu_2O_2]^{2+}$ core over the arene was the rate determining step, while the second step being barrierless or quasi-barrierless. This result reproduces the experimental observation of the phenolate-Cu_2O_2 adduct as the last spectroscopically detectable intermediate.

The electrophilic character of the rate determining step was elucidated by means of an experimental Hammett plot. Analysis of frontier molecular orbitals for the substrates further confirm the electrophilic nature of the reaction.

An Eyring plot experiment for 2-fluorophenolate as substrate showed fully agreement with calculations ($\Delta G^{\ddagger}_{exp}$ =11.8 kcal·mol^{-1}; $\Delta G^{\ddagger}_{calc}$ =11.7 kcal·mol^{-1}). The experimental chemoselectivity was rationalized on the basis of relative activation energy differences between C–F, C–H and C–Cl activations. In all cases, the *ortho* C–F bond is kinetically preferred over the other possible *ortho* bond (either C–Cl or C–H) explaining the observed chemoselectivity for $[Cu_2(O)_2(DBED)_2]^{2+}$ catalyst.

The identification of the **O** isomer as the active species and the rationalization of the chemoselectivity that $[Cu_2O_2]^{2+}$ species present over specific substrates may facilitate the design of more efficient systems, eventually catalytic and may also broaden their scope of applications. Due to the bioinspired nature of such catalysts, they can be understood as simplified (bio)models, and therefore their relatively easy study and understanding is also helpful to acquire greater knowledge on the behavior of bigger systems such as ubiquitous copper-based metalloproteins.

ASSOCIATED CONTENT

Instrumentation, materials, synthesis of $[Cu^{I}(DBED)](SbF_6)$, preparation and reactivity of Cu_2O_2 species for UV/Vis experiments, generation of $[Cu^{II}_2(\mu\text{-}\eta^2\text{:}\eta^2\text{-}O_2)(DBED)_2]^{2+}$ (**1P**) monitored by UV/Vis spectroscopy, generation of $[Cu^{III}_2(\mu\text{-}O)_2(DBED)_2]^{2+}$ (**2O**) and reactivity with 2-fluorophenolates monitored by UV/Vis spectroscopy, Hammett plot preparation, Eyring plot preparation, analysis and quantification of the final oxidized products for C-H vs C-F activation, noncovalent interaction (NCI) plots for the intermediates and DFT optimized structures are available free of charge via the Internet at http://pubs.acs.org

AUTHOR INFORMATION

Corresponding Author

* E-mail for M.C.: miquel.costas@udg.edu
* E-mail for A.C.: anna.company@udg.edu
* E-mail for J.M.L.: josepm.luis@udg.edu

ORCID

Pau Besalú-Sala: 0000-0002-0955-9762
Carla Magallón: 0000-0001-6425-5238
Miquel Costas: 0000-0001-6326-8299
Anna Company: 0000-0003-4845-4418
Josep M. Luis: 0000-0002-2880-8680

Author Contributions

P. B.-S. performed all the calculations, C.M. carried out all the experiments, and both wrote the first draft of the manuscript. M.C., A. C. and J. M. L. designed and supervised the project and co-wrote the manuscript. All authors have contributed to the analysis of the results, and they all gave approval to the final version of the manuscript. ‡ P. B-S. and C.M. contributed equally to this work.

ACKNOWLEDGMENT

This work was supported with funds from the Spanish government MICINN (PGC2018-098212-B-C22 to JML, PGC2018-101737-B-I00 to M.C., CTQ2016-77989-P to A.C.), and the Generalitat de Catalunya (2017SGR39 to J.M.L, 2017 SGR 00264 and ICREA Academia to M.C. and A.C.). We thank the Spanish government for the predoctoral grant to P.B.-S. (FPU17/02058). We are also grateful for the computational time financed by the Consorci de Serveis Universitaris de Catalunya (CSUC).

REFERENCES

1. Lemal, D. M., Perspective on Fluorocarbon Chemistry. *J. Org. Chem.* **2004,** *69* (1), 1-11.
2. Smart, B. E., Fluorine substituent effects (on bioactivity). *J. Fluor. Chem.* **2001,** *109* (1), 3-11.
3. Müller, K.; Faeh, C.; Diederich, F., Fluorine in Pharmaceuticals: Looking Beyond Intuition. *Science* **2007,** *317* (5846), 1881-1886.
4. Houde, M.; Martin, J. W.; Letcher, R. J.; Solomon, K. R.; Muir, D. C. G., Biological Monitoring of Polyfluoroalkyl Substances: A Review. *Environ. Sci. Technol.* **2006,** *40* (11), 3463-3473.
5. Key, B. D.; Howell, R. D.; Criddle, C. S., Fluorinated Organics in the Biosphere. *Environ. Sci. Technol.* **1997,** *31* (9), 2445-2454.
6. Bondar, V. S.; Boersma, M. G.; Golovlev, E. L.; Vervoort, J.; Van Berkel, W. J. H.; Finkelstein, Z. I.; Solyanikova, I. P.; Golovleva, L. A.; Rietjens, I. M., ^{19}F NMR study on the biodegradation of fluorophenols by various Rhodococcus species. *Biodegradation* **1998,** *9* (6), 475-486.
7. Peelen, S.; Rietjens, I. M.; Boersma, M. G.; Vervoort, J., Conversion of phenol derivatives to hydroxylated products by phenol hydroxylase from Trichosporon cutaneum. A comparison of regioselectivity and rate of conversion with calculated molecular orbital substrate characteristics. *Eur. J. Biochem.* **1995,** *227* (1-2), 284-291.
8. Osborne, R. L.; Raner, G. M.; Hager, L. P.; Dawson, J. H., C. fumago Chloroperoxidase is also a Dehaloperoxidase: Oxidative Dehalogenation of Halophenols. *J. Am. Chem. Soc.* **2006,** *128* (4), 1036-1037.
9. Battaini, G.; Monzani, E.; Casella, L.; Lonardi, E.; Tepper, A. W. J. W.; Canters, G. W.; Bubacco, L., Tyrosinase-catalyzed Oxidation of Fluorophenols. *J. Biol. Chem.* **2002,** *277* (47), 44606-44612.
10. Spada, A.; Palavicini, S.; Monzani, E.; Bubacco, L.; Casella, L., Trapping tyrosinase key active intermediate under turnover. *Dalton Trans.* **2009,** (33), 6468-6471.
11. Serrano-Plana, J.; Garcia-Bosch, I.; Miyake, R.; Costas, M.; Company, A., Selective Ortho-Hydroxylation–Defluorination of 2-Fluorophenolates with a Bis(μ-oxo)dicopper(III) Species. *Angew. Chem. Int. Ed. Engl.* **2014,** *53* (36), 9608-9612.
12. Mirica, L. M.; Vance, M.; Rudd, D. J.; Hedman, B.; Hodgson, K. O.; Solomon, E. I.; Stack, T. D. P., Tyrosinase Reactivity in a Model Complex: An Alternative Hydroxylation Mechanism. *Science* **2005,** *308* (5730), 1890-1892.
13. Mirica, L. M.; Vance, M.; Rudd, D. J.; Hedman, B.; Hodgson, K. O.; Solomon, E. I.; Stack, T. D. P., A Stabilized μ-η^2:η2 Peroxodicopper(II) Complex with a Secondary Diamine Ligand and Its Tyrosinase-like Reactivity. *J. Am. Chem. Soc.* **2002,** *124* (32), 9332-9333.
14. Itoh, S.; Kumei, H.; Taki, M.; Nagatomo, S.; Kitagawa, T.; Fukuzumi, S., Oxygenation of Phenols to Catechols by A (μ-η^2:η^2-Peroxo)dicopper(II) Complex: Mechanistic Insight into the Phenolase Activity of Tyrosinase. *J. Am. Chem. Soc.* **2001,** *123* (27), 6708-6709.
15. Company, A.; Palavicini, S.; Garcia-Bosch, I.; Mas-Ballesté, R.; Que Jr., L.; Rybak-Akimova, E. V.; Casella, L.; Ribas, X.; Costas, M., Tyrosinase-Like Reactivity in a $Cu^{III}_2(\mu\text{-}O)_2$ Species. *Chem. Eur. J.* **2008,** *14* (12), 3535-3538.
16. de Ruiter, G.; Thompson, N. B.; Takase, M. K.; Agapie, T., Intramolecular C–H and C–F Bond Oxygenation Mediated by a Putative Terminal Oxo Species in Tetranuclear Iron Complexes. *J. Am. Chem. Soc.* **2016,** *138* (5), 1486-1489.
17. Carsch, K. M.; de Ruiter, G.; Agapie, T., Intramolecular C–H and C–F Bond Oxygenation by Site-Differentiated Tetranuclear Manganese Models of the OEC. *Inorg. Chem.* **2017,** *56* (15), 9044-9054.
18. de Ruiter, G.; Carsch, K. M.; Takase, M. K.; Agapie, T., Selectivity of C−H versus C−F Bond Oxygenation by Homo- and Heterometallic Fe_4, Fe_3Mn, and Mn_4 Clusters. **2017,** *23* (45), 10744-10748.
19. Colomban, C.; Kudrik, E. V.; Afanasiev, P.; Sorokin, A. B., Catalytic Defluorination of Perfluorinated Aromatics under Oxidative Conditions Using N-Bridged Diiron Phthalocyanine. *J. Am. Chem. Soc.* **2014,** *136* (32), 11321-11330.
20. Sahu, S.; Quesne, M. G.; Davies, C. G.; Dürr, M.; Ivanović-Burmazović, I.; Siegler, M. A.; Jameson, G. N. L.; de Visser, S. P.; Goldberg, D. P., Direct Observation of a Nonheme Iron(IV)–Oxo Complex That Mediates Aromatic C–F Hydroxylation. *J. Am. Chem. Soc.* **2014,** *136* (39), 13542-13545.
21. Colomban, C.; Tobing, A. H.; Mukherjee, G.; Sastri, C. V.; Sorokin, A. B.; de Visser, S. P., Mechanism of Oxidative Activation of Fluorinated Aromatic Compounds by N-Bridged Diiron-Phthalocyanine: What Determines the Reactivity? *Chem. Eur. J.* **2019,** *25* (63), 14320-14331.
22. Liu, Y. F.; Yu, J. G.; Siegbahn, P. E. M.; Blomberg, M. R. A., Theoretical Study of the Oxidation of Phenolates by the $[Cu_2O_2(N,N'\text{-di-tert-butylethylenediamine})_2]^{2+}$ Complex. *Chem. Eur. J.* **2013,** *19* (6), 1942-1954.
23. Qayyum, M. F.; Sarangi, R.; Fujisawa, K.; Stack, T. D. P.; Karlin, K. D.; Hodgson, K. O.; Hedman, B.; Solomon, E. I., L-Edge X-ray Absorption Spectroscopy and DFT Calculations on Cu_2O_2 Species: Direct Electrophilic Aromatic Attack by Side-on Peroxo Bridged Dicopper(II) Complexes. *J. Am. Chem. Soc.* **2013,** *135* (46), 17417-17431.
24. Güell, M.; Luis, J. M.; Solà, M.; Siegbahn, P. E. M., Theoretical study of the hydroxylation of phenolates by the $Cu_2O_2(N,N'\text{-dimethylethylenediamine})_2^{2+}$ complex. *J. Biol. Inorg. Chem.* **2009,** *14* (2), 229-242.
25. Op't Holt, B. T.; Vance, M. A.; Mirica, L. M.; Heppner, D. E.; Stack, T. D. P.; Solomon, E. I., Reaction Coordinate of a Functional Model of Tyrosinase: Spectroscopic and Computational Characterization. *J. Am. Chem. Soc.* **2009,** *131* (18), 6421-6438.
26. Cramer, C. J.; Kinal, A.; Włoch, M.; Piecuch, P.; Gagliardi, L., Theoretical Characterization of End-On and Side-On Peroxide Coordination in Ligated Cu_2O_2 Models. *J. Phys. Chem. A* **2006,** *110* (40), 11557-11568.
27. Cramer, C. J.; Włoch, M.; Piecuch, P.; Puzzarini, C.; Gagliardi, L., Theoretical Models on the Cu_2O_2 Torture Track: Mechanistic Implications for Oxytyrosinase and Small-Molecule Analogues. *J. Phys. Chem. A* **2006,** *110* (5), 1991-2004.
28. Siegbahn, P. E. M., A comparison of the thermodynamics of O–O bond cleavage for dicopper complexes in enzymes and synthetic systems. *J. Biol. Inorg. Chem.* **2003,** *8* (5), 577-585.
29. Siegbahn, P. E. M.; Wirstam, M., Is the Bis-μ-Oxo Cu_2(III,III) State an Intermediate in Tyrosinase? *J. Am. Chem. Soc.* **2001,** *123* (47), 11819-11820.
30. Gherman, B. F.; Cramer, C. J., Quantum chemical studies of molecules incorporating a $Cu_2O_2^{2+}$ core. *Coord. Chem. Rev.* **2009,** *253* (5), 723-753.
31. Liakos, D. G.; Guo, Y.; Neese, F., Comprehensive Benchmark Results for the Domain Based Local Pair Natural Orbital

Coupled Cluster Method (DLPNO-CCSD(T)) for Closed- and Open-Shell Systems. *J. Phys. Chem. A* **2020,** *124* (1), 90-100.

32. Goerigk, L.; Hansen, A.; Bauer, C.; Ehrlich, S.; Najibi, A.; Grimme, S., A look at the density functional theory zoo with the advanced GMTKN55 database for general main group thermochemistry, kinetics and noncovalent interactions. *Phys. Chem. Chem. Phys.* **2017,** *19* (48), 32184-32215.

34. Sparta, M.; Neese, F., Chemical applications carried out by local pair natural orbital based coupled-cluster methods. *Chem. Soc. Rev.* **2014,** *43* (14), 5032-5041.

33. Comba, P.; Faltermeier, D.; Krieg, S.; Martin, B.; Rajaraman, G., Spin state and reactivity of iron(iv)oxido complexes with tetradentate bispidine ligands. *Dalton Trans.* **2020,** *49* (9), 2888-2894.

35. M. J. Frisch, G. W. Trucks, H. B. Schlegel, G. E. Scuseria, M. A. Robb, J. R. Cheeseman, G. Scalmani, V. Barone, B. Mennucci, G. A. Petersson, H. Nakatsuji, M. Caricato, X. Li, H. P. Hratchian, A. F. Izmaylov, J. Bloino, G. Zheng, J. L. Sonnenberg, M. Hada, M. Ehara, K. Toyota, R. Fukuda, J. Hasegawa, M. Ishida, T. Nakajima, Y. Honda, O. Kitao, H. Nakai, T. Vreven, J. A. Montgomery, Jr., J. E. Peralta, F. Ogliaro, M. Bearpark, J. J. Heyd, E. Brothers, K. N. Kudin, V. N. Staroverov, T. Keith, R. Kobayashi, J. Normand, K. Raghavachari, A. Rendell, J. C. Burant, S. S. Iyengar, J. Tomasi, M. Cossi, N. Rega, J. M. Millam, M. Klene, J. E. Knox, J. B. Cross, V. Bakken, C. Adamo, J. Jaramillo, R. Gomperts, R. E. Stratmann, O. Yazyev, A. J. Austin, R. Cammi, C. Pomelli, J. W. Ochterski, R. L. Martin, K. Morokuma, V. G. Zakrzewski, G. A. Voth, P. Salvador, J. J. Dannenberg, S. Dapprich, A. D. Daniels, O. Farkas, J. B. Foresman, J. V. Ortiz, J. Cioslowski, and D. J. Fox *Gaussian 09, Revision E.01*, Gaussian Inc: 2015.

36. Zhao, Y.; Truhlar, D. G., A new local density functional for main-group thermochemistry, transition metal bonding, thermochemical kinetics, and noncovalent interactions. *J. Chem. Phys.* **2006,** *125* (19), 194101.

37. Francl, M. M.; Pietro, W. J.; Hehre, W. J.; Binkley, J. S.; Gordon, M. S.; DeFrees, D. J.; Pople, J. A., Self-consistent molecular orbital methods. XXIII. A polarization-type basis set for second-row elements. *J. Chem. Phys.* **1982,** *77* (7), 3654-3665.

38. Krishnan, R.; Binkley, J. S.; Seeger, R.; Pople, J. A., Self-consistent molecular orbital methods. XX. A basis set for correlated wave functions. *J. Chem. Phys.* **1980,** *72* (1), 650-654.

39. Fukui, K., The path of chemical reactions - the IRC approach. *Acc. Chem. Res.* **1981,** *14* (12), 363-368.

40. Page, M.; Doubleday, C.; McIver, J. W., Following steepest descent reaction paths. The use of higher energy derivatives with ab initio electronic structure methods. *J. Chem. Phys*. **1990,** *93* (8), 5634-5642.

41. Dunning, T. H., Gaussian basis sets for use in correlated molecular calculations. I. The atoms boron through neon and hydrogen. *J. Chem. Phys.* **1989,** *90* (2), 1007-1023.

42. Kendall, R. A.; Dunning, T. H.; Harrison, R. J., Electron affinities of the first-row atoms revisited. Systematic basis sets and wave functions. *J. Chem. Phys.* **1992,** *96* (9), 6796-6806.

43. Marenich, A. V.; Cramer, C. J.; Truhlar, D. G., Universal Solvation Model Based on Solute Electron Density and on a Continuum Model of the Solvent Defined by the Bulk Dielectric Constant and Atomic Surface Tensions. *J. Phys. Chem. B* **2009,** *113* (18), 6378-6396.

44. Yamaguchi, K.; Jensen, F.; Dorigo, A.; Houk, K. N., A spin correction procedure for unrestricted Hartree-Fock and Møller-Plesset wavefunctions for singlet diradicals and polyradicals. *Chem. Phys. Lett.* **1988,** *149* (5), 537-542.

45. Postils, V.; Company, A.; Solà, M.; Costas, M.; Luis, J. M., Computational Insight into the Mechanism of Alkane Hydroxylation by Non-heme Fe(PyTACN) Iron Complexes. Effects of the Substrate and Solvent. *Inorg. Chem.* **2015,** *54* (17), 8223-8236.

46. Neese, F., The ORCA program system. *Wiley Interdiscip. Rev. Comput. Mol. Sci.* **2012,** *2* (1), 73-78.

47. Contreras-García, J.; Johnson, E. R.; Keinan, S.; Chaudret, R.; Piquemal, J.-P.; Beratan, D. N.; Yang, W., NCIPLOT: A Program for Plotting Noncovalent Interaction Regions. *J. Chem. Theory Comput.* **2011,** *7* (3), 625-632.

48. Johnson, E. R.; Keinan, S.; Mori-Sánchez, P.; Contreras-García, J.; Cohen, A. J.; Yang, W., Revealing Noncovalent Interactions. *J. Am. Chem. Soc.* **2010,** *132* (18), 6498-6506.

49. Company, A.; Lamata, D.; Poater, A.; Solà, M.; Rybak-Akimova, E. V.; Que, L.; Fontrodona, X.; Parella, T.; Llobet, A.; Costas, M., O_2 Chemistry of Dicopper Complexes with Alkyltriamine Ligands. Comparing Synergistic Effects on O_2 Binding. *Inorg. Chem.* **2006,** *45* (14), 5239-5241.

For table of contents only.

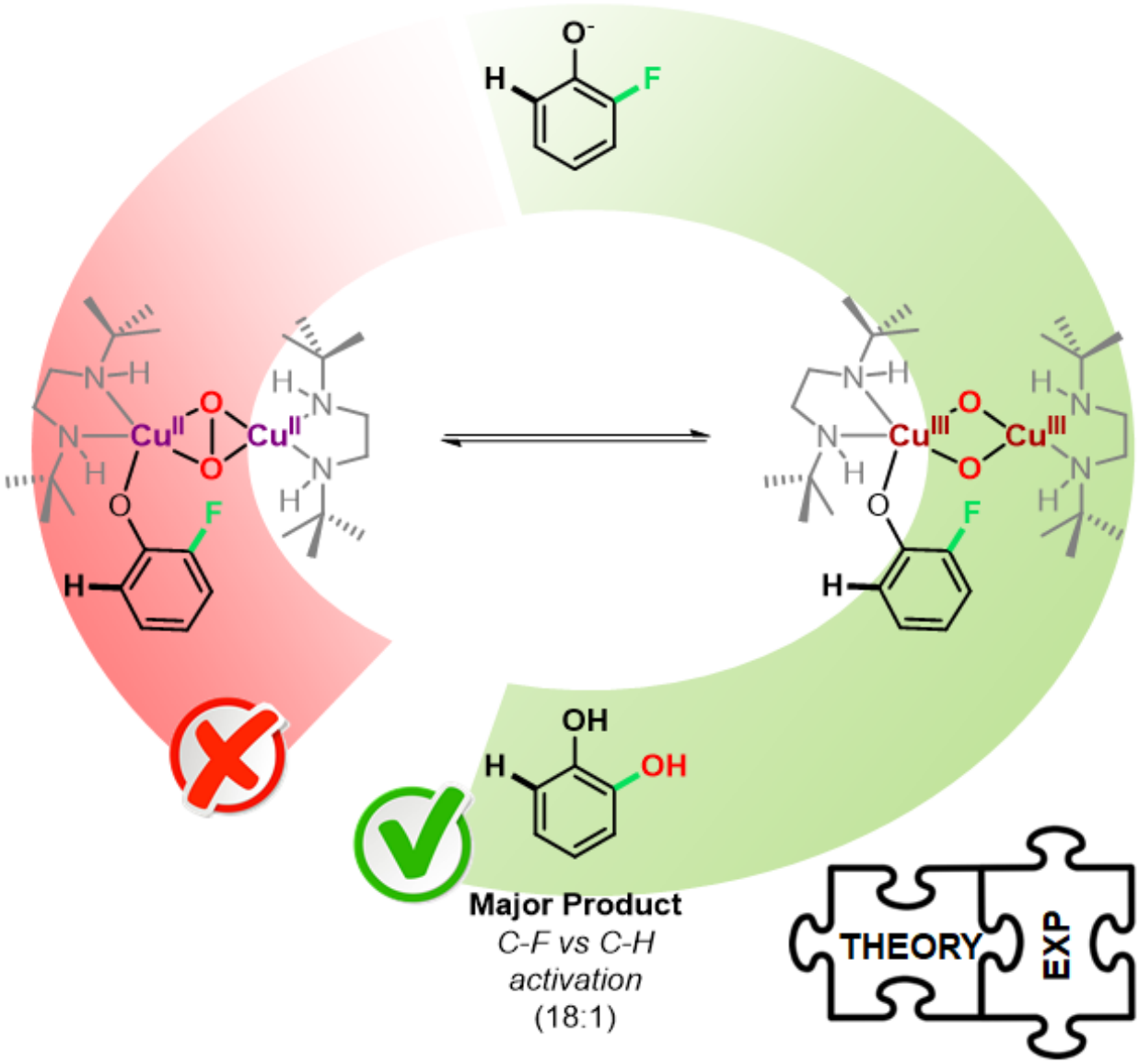

The equilibrium between (side-on)peroxo (**P**) and bis(μ-oxo) (**O**) isomers is essential to understand the *ortho*-defluorination-hydroxylation of 2-halophenolates promoted by the $[Cu_2(O)_2(DBED)_2]^{2+}$ complex. The coordination of the phenolic substrate shifts the equilibrium from **P** to **O**, which is the reactive species. We have also rationalized the chemoselective preference of $[Cu_2(O)_2(DBED)_2]^{2+}$ catalyst for the C–F activation over C–Cl and C–H activations.